We are IntechOpen, the world's leading publisher of Open Access books
Built by scientists, for scientists

6,900
Open access books available

185,000
International authors and editors

200M
Downloads

154
Countries delivered to

Our authors are among the

TOP 1%
most cited scientists

12.2%
Contributors from top 500 universities

CLARIVATE ANALYTICS
BOOK CITATION INDEX
INDEXED

WEB OF SCIENCE™

Selection of our books indexed in the Book Citation Index
in Web of Science™ Core Collection (BKCI)

Interested in publishing with us?
Contact book.department@intechopen.com

Numbers displayed above are based on latest data collected.
For more information visit www.intechopen.com

The Effect of Elemental Composition and Nanostructure of Multilayer Composite Coatings on Their Tribological Properties at Elevated Temperatures

Alexey Vereschaka, Sergey Grigoriev, Vladimir Tabakov,
Mars Migranov, Nikolay Sitnikov, Filipp Milovich,
Nikolay Andreev and Caterine Sotova

Abstract

The chapter discusses the tribological properties of samples with multilayer composite nanostructured Ti-TiN-(Ti,Cr,Al,Si)N, Zr-ZrN-(Nb,Zr,Cr,Al)N, and Zr-ZrN-(Zr,Al,Si)N coatings, as well as Ti-TiN-(Ti,Al,Cr)N, with different values of the nanolayer period λ. The relationship between tribological parameters, a temperature varying within a range of 20–1000°C, and λ was investigated. The studies have found that the adhesion component of the coefficient of friction (COF) varies nonlinearly with a pronounced extremum depending on temperature. The value of λ has a noticeable influence on the tribological properties of the coatings, and the nature of the mentioned influence depends on temperature. The tests found that for the coatings with all studied values of λ, an increase in temperature first caused an increase and then a decrease in COF.

Keywords: physical vapor deposition (PVD) coatings, coefficient of friction, tool life, thermo stability, nanolayers

1. Introduction

The tribological properties are among the most important mechanical characteristics of the coatings, affecting their performance parameters and working efficiency of products. Due to the fact that the coating characteristics vary noticeably with an increase in temperature and often differ radically from the parameters measured at room temperature [1–4], the investigation of the tribological properties at temperatures corresponding to the operating temperature (for example, a temperature in the cutting area during the study of the properties of coatings for cutting tools) is essential. The modern trends in improving the coating properties largely imply more complicated architecture and elemental composition [3–8].

Coatings are being developed with a nanolayer architecture, characterized by a number of significant advantages compared to traditional monolithic coatings [3, 6–8]. In particular, the studies detect improved crack and impact resistance of the coatings with a nanolayer architecture [9–13]. The influence of a nanolayer structure of the coating on its tribological properties is of great importance. The studies have found that the coatings with a nanolayer structure are characterized by a reduced COF, high hardness, and a low level of residual stresses [6], while with a decrease in a thickness of the binary nanolayer λ, the COF decreases and the wear resistance increases [8]. The investigation has also demonstrated that a decrease in the nanolayer period λ leads to an increase in hardness, a decrease in the COF, and an improvement in the resistance to the failure of cohesive bonds between nanolayers [14–17]. In particular, in [15], the studies of the TiAlCN/VCN nanostructured coating with λ = 2.2 nm have found that for this coating, the COF grows with an increase in temperature up to 200°C, but begins to decrease at temperatures above 650°C. The experiments found a decrease in the COF for the CrAlYN/CrN nanolayer coating with λ = 4.2 nm with an increase in temperature up to 650°C [16]. The study of the Ti/TiAlN/TiAlCN nanolayer coating detected its low COF and high wear resistance [17]. The tribological properties of the TiAlN/CNx nanostructured coating with λ = 7 nm were considered in [18]. The tests have found that the TiAlN/CNx nanostructured coating is characterized by small grain sizes and lower surface roughness in comparison with a monolithic coating of a similar composition and also by a lower COF and higher wear resistance.

The influence of the elemental composition of the coatings on their tribological properties was also investigated. The experiments revealed the COF value at room temperature for the coatings of TiN (0.55), TiCN (0.40), TiAlN (0.50), AlTiN (0.7), as well as AlTiN/Si_3N_4 consisting of AlTiN nanoparticles embedded into amorphous Si_3N_4 matrix (0.45) [19]. During the studies focused on the TiAlCrN/TiAlYN and TiAlN/VN coatings, Hovsepian et al. [20] found that the introduction of Y in the coating composition led to a decrease in the COF from 0.9 up to 0.65 during the tests conducted at temperatures ranging from 850 to 950°C. For the TiAlCrN coating, the COF was 1.1–1.6 (at temperatures of 600–900°C), while for the TiAlN/VN coating, the COF was 0.5 (at 700°C). Mo et al. [21] found that the COF of the AlCrN and TiAlN coatings was 0.75 and 0.85, respectively. With an increase in the Cr content in the CrAlN coating, a slight increase in the COF was detected [22]. Nohava et al. [23] studied the properties of the AlCrN, AlCrON, and α-$(Al,Cr)_2O_3$ coatings in comparison with the properties of the TiN-AlTiN reference coating at temperatures of 24, 600, and 800°C. The maximum value of the COF was detected at a temperature of 600°C for all the studied samples, while at a temperature of 800°C, there was a significant decrease in the COF (to 0.6–0.8) to the values lower than those detected at a room temperature (0.3–0.5). Bao et al. [24] found that for the TiCN/TiC/TiN coating, the COF was 0.4–0.5 at a room temperature and 0.6–0.7 – at a temperature of 550°C.

Thus, it can be asserted that:

- for coated products, the COF varies significantly with an increasing temperature;

- in general, the above variation of the COF is initially characterized by its gradual increase with a growth of temperature and then by its more significant decrease with a further increase in temperature;

- the parameters of the nanolayer structure (in particular, the value of the nanolayer period λ) have a noticeable influence on the COF variation.

2. Experimental

2.1 Coating deposition

Coatings were deposited through the filtered cathodic vacuum arc deposition (FCVAD) [5, 7, 25–29] technology. The experiments were carried out using a unit VIT-2, (IDTI RAS – MSTU STANKIN, Russia) with two arc evaporators with a pulsed magnetic field and one arc evaporator with filtering the vapor-ion flow. Furthermore, the complex also included a source of pulsed bias voltage supply to a substrate, a dynamic gas mixing system for reaction gases, a system to control automatically the chamber pressure and a process temperature control system, and a system for stepless adjustment of planetary gear rotation.

Two groups of samples were manufactured:

Group I included samples with three coatings of various compositions, i.e. I-a – Ti-TiN-(Ti,Cr,Al,Si)N coating; I-b – Zr-ZrN-(Nb,Zr,Cr,Al)N coating; I-c – Zr-ZrN-(Zr,Al,Si)N coating.

Group II included samples with the Ti-TiN-(Ti,Al,Cr)N coatings with different values of the nanolayer period λ, formed through varying the turntable rotation frequency n (see **Table 1**).

2.2 Measurement of tribological parameters

During the friction process, a complex system is formed in the actual contact areas. This system possesses a number of specific properties which differ from the properties of the contacting body materials when considered separately, without contact during friction. Apparently, to obtain reliable data correlating with the main factors of friction and wear, it is necessary to assess the properties of the contact area directly. However, there are several reasons which make it difficult to measure the tribological parameters directly during the operation of actual products at elevated temperature of the contact forces. Some specific features of the above-mentioned reasons are as follows:

- forces and temperatures on the contact area are distributed unevenly,

- there is a difficulty in determining the actual contact loads due to the differences in chemical purity and discreteness of contact of the contacting surfaces.

It should be noted that while two surfaces are sliding, the tangential contact force is being affected not only by shear strength of adhesive bonds, but also the deformation component of the friction force [30]. The contacting surfaces (especially those subject to wear) can have significant roughness and be heterogeneous in their physical and mechanical properties due to the polycrystalline structure. Thus, the deformation component of the tangential contact force can have a significant influence on the tribological properties of products, but its direct determination in

Sample	II-a	II-b	II-c	II-d	II-e
Turntable rotation frequency n, min^{-1}	0.25	1	1.5	5	7
Nanolayer period λ, nm	302	70	53	16	10

Table 1.
The samples depending on the turntable rotation frequency.

the friction process is associated with significant difficulties [30]. It is practically impossible to separate the deformation component from the total tangential forces and thus obtain an adhesion component, especially at an elevated contact temperature, and that fact makes it almost impossible to determine the strength of adhesive bonds immediately during the process of metal cutting [31].

Based on the above, it is physical modeling, which makes it possible to determine the tribological characteristics under conditions most closely simulating the conditions of the cutting area, is the most accurate and effective way to find the indicators of the adhesive interaction between the tool and the material being machined.

The proposed method is based on a physical model [25] (**Figure 1**), which reflects with sufficient accuracy the actual conditions of friction and wear at a local contact in the cutting area. In accordance with this model, a spherical indenter 2 made of a coated tool material (imitating an individual asperity of a contact spot of solids subject to friction), compressed by two plane-parallel counterbodies 1 made of the material being machined (with high precision and cleanliness of the contacting surfaces) rotates under load around its own axis. The force F_{exp}, spent on the rotation of the indenter and applied to the cable 3, laid in a groove of the disk 4, is mainly related to the shear strength τnn of adhesive bonds.

The shear strength τ_n of adhesive bonds is found as follows:

$$\tau_n = \frac{3}{4} \frac{F_{exp}}{\pi} \frac{R_{exp}}{r_{ind}^3} \qquad (1)$$

where F_{exp} is the circumferential force on the disc, rotating the indenter;
R_{exp} is the radius of the disk in which the indenter is fixed; and.
r_{ind} is the radius of the indent on the samples.

Due to the small dimension of the indenter, it possible to make an assumption about the normal stresses acting on the sphere surface as constant and equal in the entire indentation area (a purely plastic contact).

The above normal stresses are determined as follows:
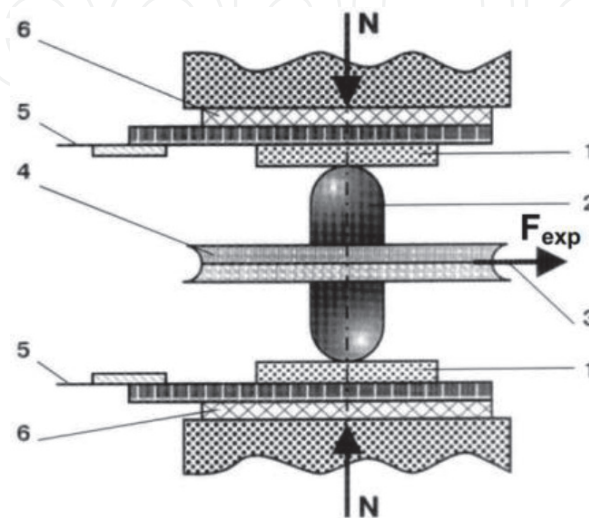
$$p_n = \frac{N}{\pi \, r_{ind}^2} \qquad (2)$$

Figure 1.
Friction contact model considered by [3, 4, 25, 31]. 1 – Two plane-parallel counterbodies; 2 – Spherical indenter; 3 – Cable; 4 – Disk; 5 – Copper plates; 6 – Thermal pads; N – Load applied.

The COF consists of two components, i.e. an adhesion component, which results from the solid body molecular interaction in the actual contact area, and a deformation component, which result from the surface layer deformation on solid bodies during the friction process [31]. In [25], the proposed model demonstrated that the forces to rotate the indenter were mainly related to the shear stress of the adhesive (interatomic and intermolecular) bonds, while in this case, no deformation component of the tangential forces was actually detected. Under the conditions of seizure, no deformation or fracture occur on the contact surface during the sliding, while the detected maximum tangential stresses reflect the hardness of near-surface layer of the softest body out of all the contacting bodies. In case when no seizure occurs, the above stresses are related to the dissipation of energy expended to break the bonds formed during the contact of the bodies.

The adhesion (molecular) component of the COF may be defined as follows:

$$f_{adh} = \frac{\tau_n}{p_n} = \frac{3}{4}\frac{F_{exp}}{N}\frac{R_{exp}}{r_{ind}}$$ (3)

where N is the load applied (N).

To apply the above method under the conditions of elevated temperatures, a special adhesiometer was developed, which allowed heating the contact area to a temperature of up to 1100°C and providing the typical temperature distribution over the depth of the contacting bodies [25]. Certain shortcomings of the above method include the relatively low rates of deformation and relative sliding. However, in terms of temperature, load, and contact cleanliness, this method is able to simulate well enough the actual conditions of friction and adhesion in the cutting area.

The indenter is a double-sided spherical cylinder with the radius of 2.5 mm and the height of 25 mm made of tool material (carbide).

After the counterbody and the indenter have been installed, the contact area is heated up to the operating temperature, and then the load N is applied, under the influence of which the indenter with the radius sphere r_1 penetrates into the counterbody surface to the depth h. Thus, the plastic contact takes place, and external friction is detected during the punch rotation [31].

The accepted loads in combination with low roughness of the contacting surfaces provide both the required area of actual contact between the indenter and the counterbody and the elimination of the formed oxide and sorbed films and the contacting of metal surfaces close to juvenile. At the same time, the oxygen penetration into the contact area is minimized due to the high density of the contact between the indenter and the counterbody. The experiments were carried out at different values of the contact temperature θ. Thus, the relationships of $\tau_n = f(p_r)$ are obtained for different values of θ. The data on the value of τ_n were obtained after the experiment had been repeated three times, with the probable deviation not exceeding 5%.

3. Results and discussion

The microstructures of the coated samples, including I-a – Ti-TiN-(Ti,Cr,Al,Si)N; I-b – Zr-ZrN-(Nb,Zr,Cr,Al)N; and I-c – Zr-ZrN-(Zr,Al,Si)N, are shown in **Figure 2**. The coatings are nanostructured, the thicknesses of the nanolayers are 30–80 nm, and the total coating thickness reaches about 3 μm.

The microstructures of the coated samples under the study are depicted in **Figure 2** [3].
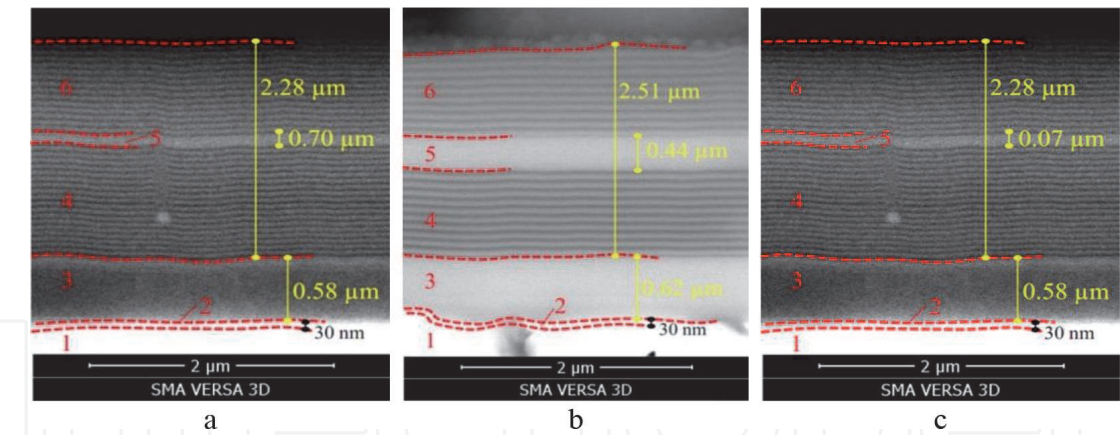
Figure 2.
The structure of the coated samples under the study. a – Ti-TiN-(Ti,Cr,Al,Si)N coating; b – Zr-ZrN-(Nb,Zr, Cr,Al)N coating; c – Zr-ZrN-(Zr,Al,Si)N coating [3]; I-c – Zr-ZrN-(Zr,Al,Si)N coating. 1 –WC-Co substrate; 2 – adhesion sublayer; 3 – transitional layer; 4 – internal zone of wear-resistant layer; 5 – intermediate sublayer; 6 – external zone of wear-resistant layer.

The results of the studies of the nanolayer coating Ti-TiN-(Ti,Al,Cr)N structure (samples of Group II) are presented in **Figure 3** [4].

As seen from **Figure 3**, all the coatings under study have a nanolayer structure. The experiments found the nanolayer thicknesses, which ranged from 10 nm to 302 nm, depending on the coating type. The earlier studies [4,34,35] revealed that each nanolayer of the II-a coating had a complex structure, formed due to the planetary rotation of the toolset during the deposition process [4, 25, 32]. In [4, 25], it is also found that the coatings with the nanolayer thicknesses of 70–10 nm also have a similar complex structure. At the same time, the nanolayers of the II-a and II-c coatings affect the formation of the crystalline structure, and the growth of crystals during the deposition is limited by the boundaries of one nanolayer. The II-d and II-e coatings demonstrate the growth of crystals, which is not limited by the nanolayer boundaries.

The experiments have been conducted at temperatures ranging from 20 to 550°C to investigate the influence of temperature on the tribotechnical properties of tribopairs in the "the material being machined–carbide with wear-resistant complex" interface (shear strength τnn of adhesive bond, normal stress on contact P_{rn}, and relation $\frac{\tau_{nn}}{P_{rn}}$, actually representing the adhesion component of the COF, on which
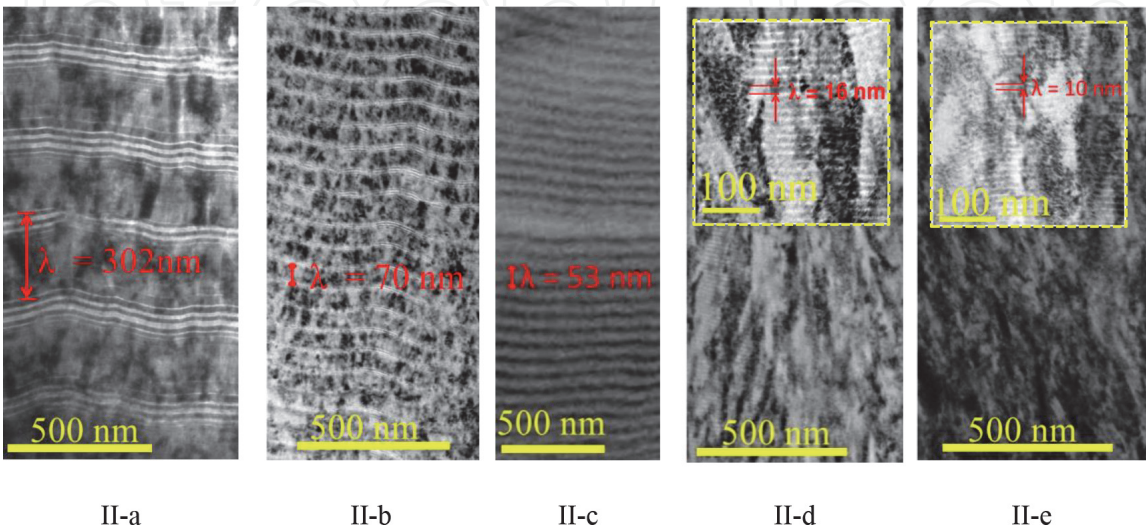

II-a	II-b	II-c	II-d	II-e

Figure 3.
The nanolayer structure of coatings on samples (TEM) [4]. a – λ = 304 nm, b - λ = 70 nm, c - λ = 53 nm, d - λ = 10 nm.

the deeper deformation of contact layers depends [F1, F2]). **Figures 4** and **5** exhibit curves reflecting the relationship between τ_{nn}, P_{rn}, $\frac{\tau_{nn}}{P_{rn}}$, and temperature. The above relationships demonstrate that the shear stresses τ_{nn} first increase for all the samples under study and then decrease with an increasing temperature. At the same time, for the sample with the Zr-ZrN-(Nb,Zr,Cr,Al)N coating, the shear stresses τ_{nn} initially grow noticeably with an increase in temperature, but when the temperature exceeds 400°C, they begin to decrease, while the process intensity grows with an increase in temperature. In particular, the conducted experiments found that at temperature of 400°C, for samples of carbide WC–Co, the parameter of τ_{nn} was significantly (almost by 2 times) higher for a sample with the Zr-ZrN-(Nb,Zr,Cr, Al)N coating compared to uncoated samples, but at temperature above 400°C, an uncoated sample demonstrated higher τnn. The samples with the Ti-TiN-(Ti,Cr,Al, Si)N coating demonstrated the lowest relationship between τnn and temperature among all the samples under the study. With an increasing temperature, τnn first increases slightly; however, when at temperatures exceeding 300°C, the parameter of τnn starts decreasing with an increase in temperature. It should be noted that at the maximum temperature of 550°C, τnn is approximately equal to τnn at room temperature.
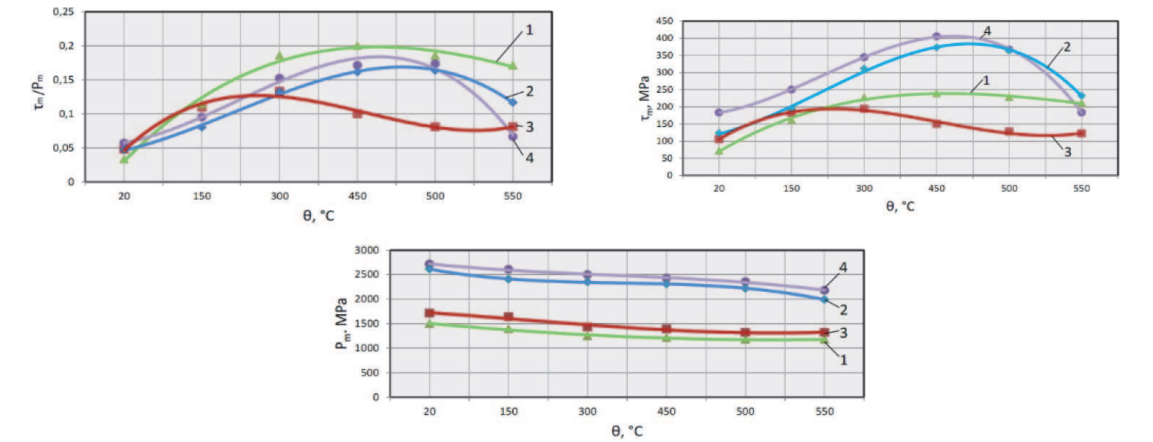

Figure 4.
Influence of temperature on tribotechnical properties of tribopair in the "steel AISI 321–carbide (WC-Co) with coating" interface [3]. 1 – Uncoated sample; 2 – Zr-ZrN-(Zr,Al)N coating; 3 –Ti-TiN-(Ti,Cr,Al,Si)N coating; 4 –Zr-ZrN-(Nb,Zr,Cr,Al)N coating.
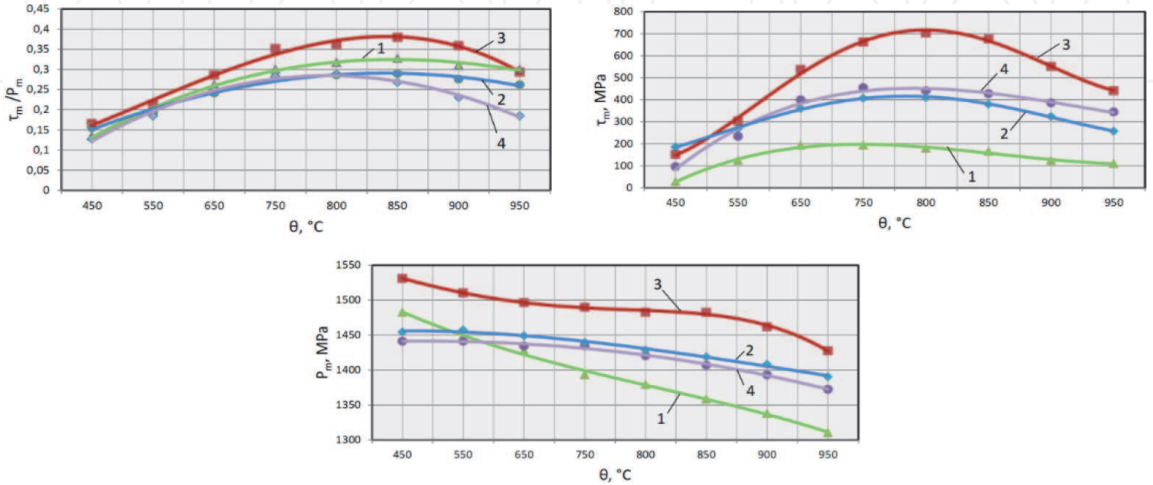

Figure 5.
Influence of temperature on tribotechnical properties of tribopair in the "steel S31600–carbide (WC-Co) with coating" interface [3]. 1 – Uncoated; 2 – Zr-ZrN-(Zr,Al)N coating; 3 – Ti-TiN-(Ti,Cr,Al,Si)N coating; 4 – Zr-ZrN-(Nb,Zr,Cr,Al)N coating.

The specific features of the variation of the adhesion (molecular) component f_{adh} of the COF with an increase in temperature were considered. Coated samples demonstrated noticeably lower values of f_{adh} compared to an uncoated sample, at all temperatures and for all types of carbides. Meanwhile, f_{adh} reaches its maximum at temperature of about 400–450°C, and after that, f_{adh} begins to decrease. The sample with the Ti-TiN-(Ti,Cr,Al,Si)N coating demonstrated the lowest value of the adhesion (molecular) component fadh of the COF. However, when the limit temperature of 550°C is reached, fadh decreases sharply for the sample with the Zr-ZrN-(Nb,Zr,Cr,Al)N coating. Thus, at temperature of 550°C, the samples with the both coatings under consideration demonstrate approximately the same values of f_{adh}, while the substantially lower value of f_{adh} was detected for the uncoated sample. The conducted experiments make it possible to predict that with a further increase in temperature, the sample with the Zr-ZrN-(Nb,Zr,Cr,Al)N coating will demonstrate the minimum value of f_{adh}.

While studying the variation of f_{adh} upon the contact with the counterbody made of S31600 steel (**Figure 5**), it is possible to notice that the dynamics of the change in f_{adh} is similar for all the samples under consideration: the value of f_{adh} first increases, but begins to decrease after a certain temperature is reached. However, for different samples, the value of f_{adh} begins to fall at different temperatures. In particular, for the sample with the ZrN-(Nb,Zr,Cr,Al)N coating, fadh begins to decrease when the temperature reaches 750°C, while for the sample with the Ti-TiN-(Ti,Cr,Al,Si)N coating – at temperature of 850°C. If upon the contact with the counterbody made of American Iron and Steel Institute (AISI) 321 steel, the sample with the Ti-TiN-(Ti,Cr,Al,Si)N coating exhibits the minimum value of f_{adh} in a range from 300 to 550°C, then upon the contact with the counterbody made of S31600 steel, the sample with the Ti-TiN-(Ti,Cr,Al,Si)N coating demonstrates the highest value of fadh among all the samples under consideration. Meanwhile, the remaining samples showed largely the same dynamics of the variation in f_{adh} for counterbodies made of the both materials under consideration.

The results of the investigation into the tribological parameters of the samples II-a – II-e are presented in **Figure 6**.

The investigation of the relationship between the tribological properties and temperature for samples with various coatings demonstrated that with an increase in temperature, the value of f_{adh} varies nonmonotonically and is of extreme nature. Within a temperature range from 500 to 800°C, an increase in the parameters of the fictional contact is related to an increase in the adhesive interaction on the contact surface. At 800°C, the adhesion on the contacting surface of friction is maximum, which can negatively affect the wear resistance of the product. The sample with the II-e coating demonstrates the higher value of f_{adh}, which begins to decrease at elevated temperatures. This phenomenon can relate to the formation of tribological oxide films (titanium and aluminum oxides), while the thicknesses of the coating layers are of key importance.

The sample with the II-d coating demonstrated the most favorable value of f_{adh}, as well as the lowest shear strength τ_n of adhesive bonds. The advantages of this coating are especially clearly demonstrated at temperatures above 600°C. It is important to note that for the samples with the minimum nanolayer thicknesses (II-d and II-e), the value of f_{adh} continuously increases up to the temperature of 800°C and then begins to noticeably decrease, and such a decline is especially clear for the II-e coating). For the coatings with large values of the nanolayer period λ (II-a, II-b, and II-c), a decrease of f_{adh} is observed at temperatures above 700°C, and such a decline intensifies with a decrease in λ. Such a decrease is least pronounced in the II-a coatings with the maximum nanolayer period λ. Thus, it can be assumed that for the coatings with the minimum value of λ (II-d and II-e), the active oxidation begins at
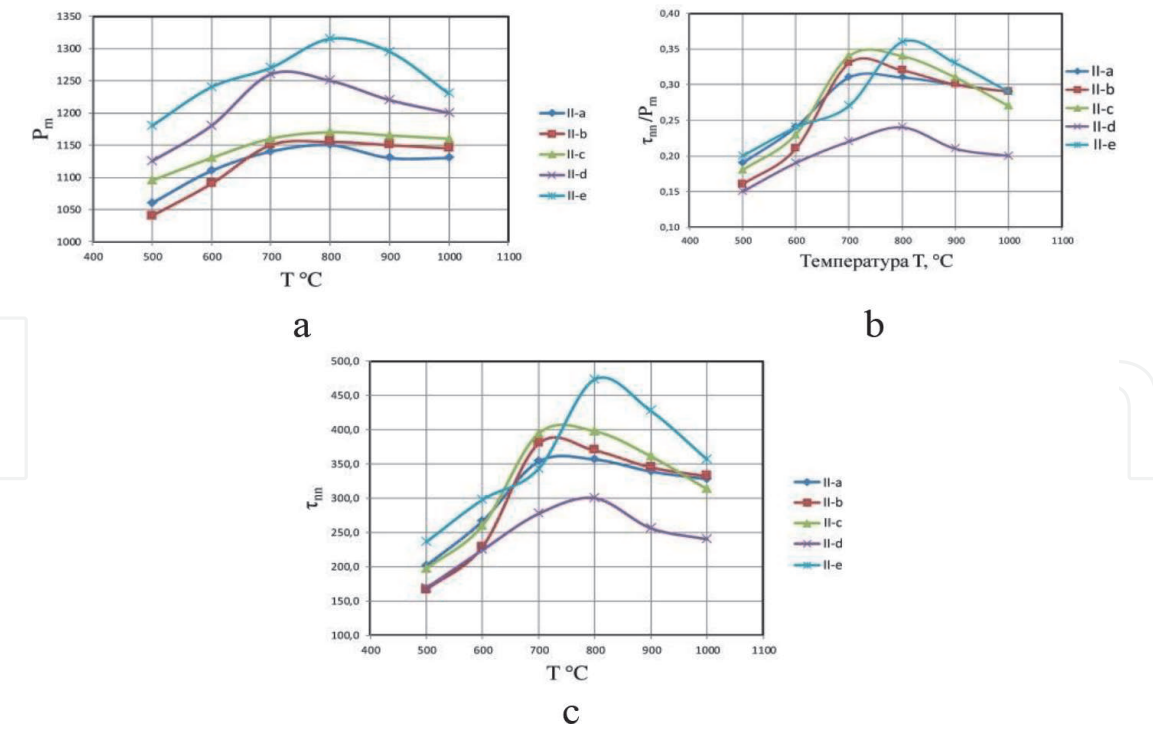
Figure 6.
The results of the investigation into the tribological properties of the samples II in the "steel AISI 1045–carbide (WC-Co) with coating" interface [4]: A – Normal stresses $\mathbf{P_{rn}}$; b – Strengths on cut $\mathbf{\tau_n}$; c – Coefficient of friction $\mathbf{f_{adh}} = \mathbf{\tau_n/P_{rn}}$.

temperatures above 800°C, while for the coatings with larger values of λ (II-a, II-b, and II-c), the oxidation processes start already at a temperature of 700°C. Thus, it can be concluded that a smaller value of λ provides better resistance to thermal oxidation, due to an increased number of interlayer interfaces inhibiting the processes of thermal destruction of the surface layer of the coating [4, 11].

There is a significant difference between the tribological characteristics of the II-d and II-e samples. In particular, when the value of λ decreases from 16 nm (II-d) to 10 nm (II-e), the value of f_{adh} increases significantly, and the most significant difference in f_{adh} is demonstrated by the II-d and II-e samples in the temperature range from 800 to 900°C. When the above temperatures are reached, the spinodal decomposition of the (Ti,Al,Cr)N phase begins, accompanied by the formation of a soft hexagonal AlN phase and also a release of pure Ti, Al and Cr [4, 11]. The interlayer interfaces can slow down the formation of the decomposition zone, although, if the value of λ is too small, this effect becomes significantly weaker, and as a result, more intense spinodal decomposition is detected for the II-e sample and less intense – for the II-d sample.

Figure 7 depicts the influence of λ on the adhesion component f_{adh} of the COF. Based on the obtained approximating curves, it is possible to distinguish two distinct extrema of f_{adh}, including the maximum in a range of λ = 70–53 nm and the minimum in a range of λ = 16–10 nm. A decrease in the value of λ from 16 to 10 nm leads to a noticeable increase in f_{adh} at all the temperatures under consideration.

Temperature has a significant influence on the value of f_{adh} and the nature of its variation depending on the value of λ. Based on the data presented in **Figure 7**, three temperature ranges can be distinguished, characterized by the different influence of the nanolayer period λ on the adhesion component f_{adh} of the COF.

When temperatures are within a range from 500 to 600°C, the influence of λ on f_{adh} is not significant, and the maximum values of f_{adh} are typical for coatings with the maximum (302 nm) and minimum (10 nm) values of λ.

At temperatures of 700–900°C, the influence of λ on fadh enhances noticeably. There is a significant decline in the value of f_{adh} with a decrease in λ from 53 to
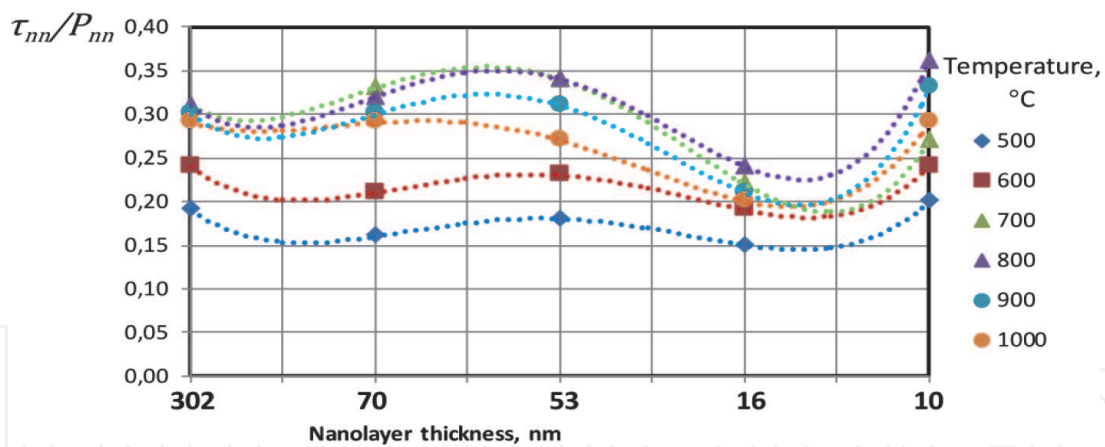
Figure 7.
Relationship between the adhesion component f$_{adh}$ of the COF and the nanolayer period λ at different temperatures [4].

16 nm, and equally significant growth is detected with a further decrease in λ from 16 to 10 nm. At a temperature of 1000°C, a decrease in λ from 302 to 16 nm leads to a continuous decrease in f_{adh} and then to a noticeable increase at λ = 10 nm.

The specified temperature ranges can be related to the temperature in the cutting area under various conditions of machining. In particular, temperatures within a range from 500 to 800°C are usually detected at relatively low cutting speeds v_c, when the mechanisms of adhesive and abrasive wear play a key role, while oxidation and diffusion processes are relatively weakly expressed [33–35]. A range of temperatures within 800–900°C is typical for significantly high cutting speeds, when oxidation and diffusion processes begin to play an important role, and the destruction of the external layers of the coating begins due to spinodal decomposition [11, 36–38]. At the same time, such elevated temperatures trigger the formation of protective oxide films, which have a positive influence on the tribological parameters of the cutting process. A range of temperatures within 900–1000°C is typical during dry cutting at the highest possible cutting speed. At the temperatures within the above range, the oxidation and diffusion processes prevail, and a coating can fail as a result of active oxidation and spinodal decomposition [11, 33–35].

Thus, at relatively low cutting speeds, the best cutting properties can be demonstrated by a tool with the II-d coating, characterized by the minimal tendency to adhesion to the material being machined in combination with the significantly high hardness, which provides good resistance to both adhesive and abrasive wear. During the cutting at high cutting speeds (and, accordingly, elevated temperatures in the cutting area), the best cutting properties can be expected from a cutting tool with the II-e coating, characterized by better resistance to oxidation and propagation of spinodal decomposition due to the maximum number of interlayer interfaces that restrain the indicated phenomena. The II-e coating is also characterized by the highest hardness. Meanwhile, a significantly high value of the adhesion component of the COF for the II-e coating can even play a positive role in the turning of difficult-to-cut materials. This effect can be associated with a decrease in the contact stresses due to an increase in the contact area of the chips with the rake face of the tool at a significantly lower intensity of the increase in the normal forces, acting on the contact area of the rake face, which in turn reduces cracking and brittle fracture in the coated tool [39]. The above assumptions were confirmed by the conducted cutting tests [3, 4]. The processes occurring in the surface layers of the coatings under the simultaneous action of elevated temperature, oxidation, and diffusion were considered in detail using the example of coating I-a – Ti-TiN-(Ti, Cr,Al,Si)N (**Figure 8**) [39]. The formation of a layer with signs of active oxidation
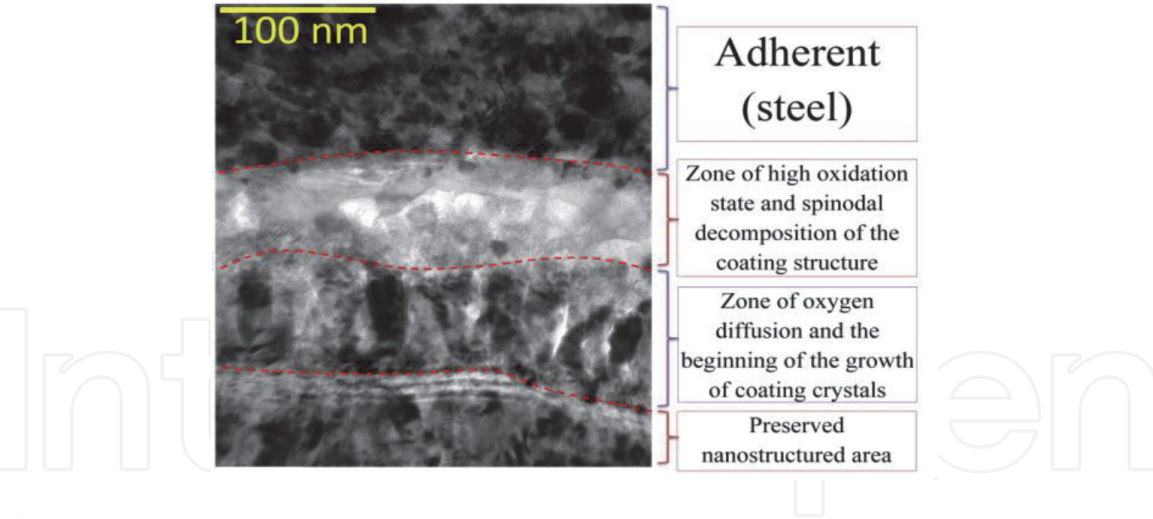
Figure 8.
Structure of the surface layers in I-a – Ti-TiN-(Ti,Cr,Al,Si)N coating at the boundary with the steel adherent (TEM) [39].

can be noticed in the interface area between the steel adherent and the coating. This layer is also characterized by the phenomenon of spinodal decomposition and active diffusion of Fe. The nanolayer structure of the coating was completely destroyed in this area. Below the mentioned layer there is a layer characterized by active growth of coating grains under the influence of the elevated temperature. This layer also contains signs of diffusion of O and Fe, but in much smaller volumes. Finally, below there is an area of the coating with the preserved nanostructure. The area demonstrates no presence of diffused Fe and O.

The study focused on the distribution of chemical elements in the area of the "coating – steel adherent" finds (see **Figure 9**) the presence of diffusing Fe in the surface layers of the coating at a depth not exceeding 200 nm and diffusing O at a depth not exceeding 300 nm from the coating surface. There is also a diffusion of Ti from the coating into the steel adherent to a depth not exceeding 100 nm. Thus, under the influence of such factors as temperature, oxidation, and diffusion of Fe, a
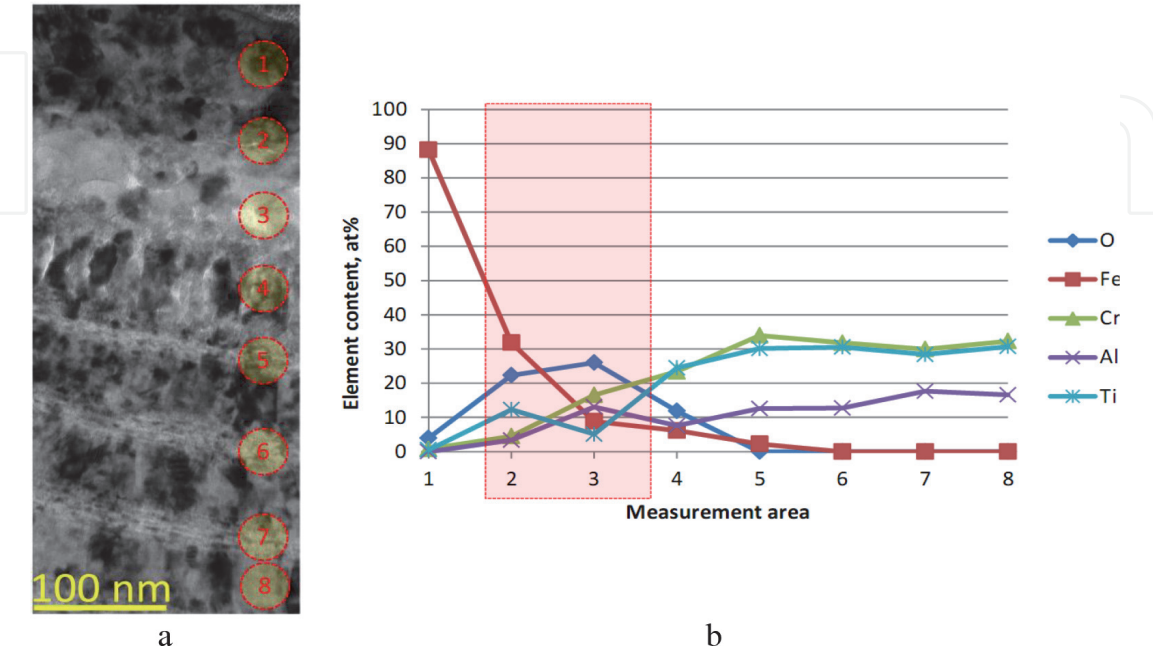

Figure 9.
Study of the oxidation layer. (a) Diagram of research areas (TEM), and (b) distribution of chemical elements by areas.

surface layer with new special properties, influencing, among other phenomena, a decrease in the value of fadh is being formed in the coating.

4. Conclusions

The processes that take place in the cutting area are very complex and difficult for modeling. Till present, there is no any ideal model (both mathematical and mechanical), which would take into account all the factors involved in the cutting process (stresses, temperature, diffusion and chemical processes, etc.), and such a model is unlikely to be created in the near future. Accordingly, an entirely adequate assessment of the working efficiency of a coating can be made only in the course of cutting tests. At the same time, there are several techniques, including those considered in this chapter, which make it possible to predict the performance properties of the coatings with a fairly high probability.

The conducted experiments found the following:

1. For the coatings under study, the adhesion (molecular) component f_{adh} of the coefficient of friction (COF) first grows with an increase in temperature and then begins to decrease noticeably with a further increase in temperature.

2. The temperature at which fadh begins to decrease depends not only on the coating material, but also on the counterbody material. In particular, for AISI 321 steel, the above temperature is 400–450°C, while for AISI 1045 and S31600 steels, it stays within a range of 800–850°C.

3. The samples with the Ti-TiN-(Ti,Cr,Al,Si)N coating showed the smallest value of f_{adh} in the temperature range under study (despite the fact that at room temperature, this value differed little from the data of other samples). The smallest change in f_{adh} at varying temperature was also detected for the samples with the Ti-TiN-(Ti,Cr,Al,Si)N coating. Meanwhile, the presence of Si in the coating composition does not have a noticeable influence on f_{adh}, because the Ti-TiN-(Ti,Al,Cr)N coating demonstrated a result similar to the results obtained during the study focused on the Ti-TiN-(Ti,Cr,Al,Si)N coating.

4. The experiments detected the influence of the nanolayer period λ of the Ti-TiN-(Ti,Al,Cr)N coating on its tribological properties. The tests found that for the coatings with all studied values of λ, an increase in temperature first caused an increase and then a decrease in f_{adh}.

5. Three temperature ranges, characterized by different influence of λ on f_{adh}, are detected. In the temperature range of 500–600°C, the influence of λ on f_{adh} is insignificant. In the temperature range of 700–800°C, the influence of λ on f_{adh} grows noticeably, and there is a gradual increase of f_{adh} with a decrease in λ from 302 to 53 nm, then noticeable decrease in f_{adh} follows a decrease in λ from 53 to 16 nm, and, again, there is a noticeable increase in fadh with a further decrease in λ from 16 to 10 nm. At temperatures of 900–1000°C, there is an almost continuous decrease in f_{adh} with a decrease in λ from 302 to 16 nm, and then a noticeable increase in f_{adh} with a further decrease in λ from 16 to 10 nm.

6. Under the simultaneous action of elevated temperature, oxidation processes, and diffusion of Fe from the steel counterbody, a surface layer with new properties is being formed in the coating, with a positive effect on the decrease in f_{adh}.

Acknowledgements

Conflict of interest

The authors declare no conflict of interest.

Author details

Alexey Vereschaka[1*], Sergey Grigoriev[2], Vladimir Tabakov[3], Mars Migranov[4], Nikolay Sitnikov[5], Filipp Milovich[6], Nikolay Andreev[6] and Caterine Sotova[2]

1 IDTI RAS, Moscow, Russia

2 Moscow State Technological University STANKIN, Moscow, Russia

3 Ulyanovsk State Technical University, Ulyanovsk, Russia

4 Ufa State Aviation Technical University, Ufa, Russia

5 National Research Nuclear University MEPhI, Moscow, Russia

6 National University of Science and Technology MISiS, Moscow, Russia

*Address all correspondence to: dr.a.veres@yandex.ru

References

[1] Navinsek B, Panjan P. Oxidation resistance of PVD Cr, Cr–N and Cr–N–O hard coatings. Surf Coat Technol 1993;59:244–8

[2] Milosev I, Strehblow H-H, Navinsek B. XPS in the study of high-temperature oxidation of CrN and TiN hard coatings. Surf Coat Technol 1995; 74–5:897–902.

[3] Vereschaka, A., Aksenenko, A., Sitnikov, N., Migranov, M., Shevchenko, S., Sotova, C., Batako, A., Andreev, N. Effect of adhesion and tribological properties of modified composite nano-structured multi-layer nitride coatings on WC-Co tools life. Tribology International 2018;128:313–327

[4] Vereschaka, A., Grigoriev, S., Tabakov, V., Migranov, M., Sitnikov, N., Milovich, F., Andreev, N. Influence of the nanostructure of Ti-TiN-(Ti,Al, Cr)N multilayer composite coating on tribological properties and cutting tool life. Tribology International 2020;150: 106388

[5] Vereshchaka, A.A., Vereshchaka, A.S., Mgaloblishvili, O., Morgan, M.N., Batako, A.D. Nano-scale multilayered-composite coatings for the cutting tools. International Journal of Advanced Manufacturing Technology 2014;72(1–4):303–317

[6] Hovsepian P.E., Ehiasarian A.P., Deeming A., Schimpf C. Novel TiAlCN/VCN nanoscale multilayer PVD coatings deposited by the combined high-power impulse magnetron sputtering/unbalanced magnetron sputtering (HIPIMS/UBM) technology. Vacuum 2008;82:1312–1317

[7] Vereschaka A.A., Tabakov V., Grigoriev S., Aksenenko A., Sitnikov N., Oganyan G., Seleznev A., Shevchenko S. Effect of adhesion and the wear-resistant layer thickness ratio on mechanical and performance properties of ZrN – (Zr,Al,Si)N coatings. Surf. Coatings Technol. 2019;357:218–234

[8] Zhang Z.G., Rapaud O., Allain N., Mercs D., Baraket M., Dong C., Coddet C. Microstructures and tribological properties of CrN/ZrN nanoscale multilayer coatings. Applied Surf. Sci. 2009;255:4020–4026

[9] Bouzakis K.D., Michailidis N., Skordaris G., Bouzakis E., Biermann D., M'Saoubi R. Cutting with coated tools: Coating technologies, characterization methods and performance optimization, CIRP Ann. Manuf. Technol. 2012;61: 703–723

[10] Zhang S., Sun D., Yongqing F., Hejun D. Recent advances of superhard nanocomposite coatings: A review, Surf. Coatings Technol. 2003;167:113–119.

[11] Vereschaka, A., Tabakov, V., Grigoriev, S., Sitnikov, N., Oganyan, G., Andreev, N., Milovich, F. Investigation of wear dynamics for cutting tools with multilayer composite nanostructured coatings in turning constructional steel. Wear 2019;420–421:17–37

[12] Vereschaka, A.A., Grigoriev, S.N., Sitnikov, N.N., Batako, A.D. Delamination and longitudinal cracking in multi-layered composite nano-structured coatings and their influence on cutting tool life. Wear 2017;390–391: 209–219

[13] Skordaris G., Bouzakis K.-D., Charalampous P., Bouzakis E., Paraskevopoulou R., Lemmer O., Bolz S. Brittleness and fatigue effect of mono- and multi-layer PVD films on the cutting performance of coated cemented carbide inserts, CIRP Ann. Manuf. Technol. 2014;63:93–96.

[14] Araujo J.A., Araujo G.M., Souza R.M., Tschiptschin A.P. Effect of

periodicity on hardness and scratch resistance of CrN/NbN nanoscale multilayer coating deposited by cathodic arc technique. Wear 2015; 330–331:469–477.

[15] Kamath G., Ehiasarian A.P., Purandare Y., Hovsepian P.E. Tribological and oxidation behaviour of TiAlCN/VCN nanoscale multilayer coating deposited by the combined HIPIMS/(HIPIMS-UBM) technique. Surf. Coatings Technol. 2011;205: 2823–2829.

[16] Hovsepian P.E., Ehiasarian A.P., Braun R., Walker J., Du H. Novel CrAlYN/CrN nanoscale multilayer PVD coatings produced by the combined high power impulse magnetron sputtering/unbalanced magnetron sputtering technique for environmental protection of γ-TiAl alloys. Surf. Coatings Technol. 2010;204:2702–2708.

[17] Al-Bukhaiti M.A., Al-Hatab K.A., Tillmann W., Hoffmann F., Sprute T. Tribological and mechanical properties of Ti/TiAlN/TiAlCN nanoscale multilayer PVD coatings deposited on AISI H11 hot work tool steel. Applied Surf. Sci. 2014;318:180–190.

[18] Wang M., Toihara T., Sakurai M., Kurosaka W., Miyake S. Surface morphology and tribological properties of DC sputtered nanoscale multilayered TiAlN/CNx coatings. Tribology Int. 2014;73:36–46.

[19] Coatings Specifications – Coating Guide [Internet], http://www.platit.com/coatings/coating-specifications

[20] Hovsepian P.E., Lewis D.B., Luo Q., Munz W.-D., Mayrhofer P.H., Mitterer C., Zhou Z., Rainforth W.M., TiAlN based nanoscale multilayer coatings designed to adapt their tribological properties at elevated temperatures. Thin Solid Films 2005; 485:160–168

[21] Mo J.L., Zhu M.H., Lei B., Leng Y. X., Huang N., Comparison of tribological behaviours of AlCrN and TiAlN coatings — Deposited by physical vapor deposition, Wear 2007;263:1423–1429

[22] Wang L., Zhang G., Wood R.J.K., Wang S.C., Xue Q., Fabrication of CrAlN nanocomposite films with high hardness and excellent anti-wear performance for gear application, Surface & Coatings Technology 2010; 204: 3517–3524.

[23] Nohava J., Dessarzin P., Karvankova P., Morstein M., Characterization of tribological behavior and wear mechanisms of novel oxynitride PVD coatings designed for applications at high temperatures, Tribology International 2015;81: 231–239.

[24] Bao M., Xu X., Zhang H., Liu X., Tian L., Zeng Z., Song Y., Tribological behavior at elevated temperature of multilayer TiCN/TiC/TiN hard coatings produced by chemical vapor deposition, Thin Solid Films 2011;520:833–836.

[25] Vereschaka A, Tabakov V, Grigoriev S, Sitnikov N, Milovich F, Andreev N, Sotova C, Kutina N. Investigation of the influence of the thickness of nanolayers in wear-resistant layers of Ti-TiN-(Ti,Cr,Al)N coating on destruction in the cutting and wear of carbide cutting tools. Surface & Coatings Technology 2020;385:125402; doi:10.1016/j.surfcoat.2020.125402

[26] Sobol'O.V., AndreevA.A., GrigorievS.N., VolosovaM.A., Gorban'V.F. Vacuum-arc multilayer nanostructured TiN/Ti coatings: structure, stress state, properties. Metal Science and Heat Treatment 2012;54(1–2):28–33

[27] Metel A., Grigoriev S., Melnik Y., Panin V., PrudnikovV. Cutting Tools Nitriding in Plasma Produced by a Fast

Neutral Molecule Beam Japanese Journal of Applied Physics. 2011;50(8):08JG04,

[28] Fominski V.Yu., Grigoriev S.N., CelisJ.P., Romanov R.I., OshurkoV.B. Structure and mechanical properties of W–Se–C/diamond-like carbon and W–Se/diamond-like carbon bi-layer coatings prepared by pulsed laser deposition. 2012;520(21):6476–6483

[29] Fominski V.Yu., Grigoriev S.N., Gnedovets A.G., Romanov R.I. Pulsed laser deposition of composite Mo-Se-Ni-C coatings using standard and shadow mask configuration, Surface and Coatings Technology, 2012;206 (24): 5046–5054

[30] Shuster L.S. Device for investigating adhesion interaction. Patent of Russia 34249 26/03/2003.

[31] Shuster L.S. Adhesive interaction of the cutting tool with the material being processed. Mashinostroenije, Moscow, 1988.

[32] Vereschaka, A.A., Bublikov, J.I., Sitnikov, N.N., Oganyan, G.V., Sotova, C.S. Influence of nanolayer thickness on the performance properties of multilayer composite nano-structured modified coatings for metal-cutting tools. International Journal of Advanced Manufacturing Technology 2018;95(5–8): 2625–2640

[33] Loladze T.N., Nature of brittle failure of cutting tool. Ann CIRP, 1975; 24(1):13–16.

[34] Boothroyd G., Knight W.A. Fundamentals of machining and machine tools, CRC Press, Boca Raton, 2006.

[35] Shaw M.C. Metal Cutting Principles, Clarendon Press, Oxford, 1989.

[36] Choi P.-P., Povstugar I., Ahn J.-P., Kostka A., Raabe D., Thermal stability of TiAlN/CrN multilayer coatings

studied by atom probe tomography. Ultramicroscopy. 2011;111(6):518–523.

[37] Povstugar I., Choi P.-P., Tytko D., Ahn J.-P., Raabe D., Interface-directed spinodal decomposition in TiAlN/CrN multilayer hard coatings studied by atom probe tomography. ActaMaterialia 2013;61:7534–7542.

[38] Barshilia H.C., Prakash M.S., Jain A., Rajam K.S., Structure, hardness and thermal stability of TiAlN and nanolayered TiAlN/CrN multilayer films, Vacuum. 2005;77(2):169–179 DOI: 10.1016/j.vacuum.2004.08.020

[39] Vereschaka A, Tabakov V, Grigoriev S, Sitnikov N, Milovich F, Andreev N, Bublikov J. Investigation of wear mechanisms for the rake face of a cutting tool with a multilayer composite nanostructured Cr-CrN-(Ti,Cr,Al,Si)N coating in high-speed steel turning. Wear 2019;438–439:203069 DOI 10.1016/j.wear.2019.203069